Angewandte Chemie
Eine Zeitschrift der Gesellschaft Deutscher Chemiker

Supporting Information

69451 Weinheim, Germany

Mixed Valence Diiron Dithiolate Model for the Hox State of the [FeFe]- Hydrogenase

Aaron K. Justice, Thomas B. Rauchfuss, Scott R. Wilson

I. Preparative Methods.

II. Spectroscopic Data.

III. Crystallography (CIF file is separate).

I. Preparative Methods.

Unless otherwise indicated, reactions were conducted using Schlenk techniques at room temperature. Unless otherwise indicated, reagents were purchased from Aldrich. Solvents were either HPLC-grade from an alumina filtration system (Glasscontour Co., Irvine, CA) or distilled under nitrogen over CaH_2. PMe_3 was obtained from Strem and distilled prior to use on a high-vacuum line

Cp_2FeBF_4 (Aldrich) was purified by recrystallization as follows: 5 grams of the commercial Cp_2FeBF_4 was extracted into ~300 mL of CH_2Cl_2. The deep blue solution was filtered to remove solids, and the filtrate was concentrated to ~150 ml (precipitate begins to appear) and then diluted with ~300 mL of hexanes. The purified solid was then extracted into ~200 mL of acetone. This solution (filtration is not needed) was concentrated to half volume and then diluted to ~300 mL with Et_2O. The blue product was isolated via filtration and dried under vacuum.

$Fe_2(S_2C_2H_4)(CO)_3(PMe_3)$(dppv) was prepared as recently described (Justice, A. K.; Zampella, G.; De Gioia, L.; Rauchfuss, T. B.; van der Vlugt, J. I.; Wilson, S. R. *Inorg. Chem.* **2007**, *46*, 1655-1664).

NMR spectra were recorded at room temperature on a Varian Mercury 500 MHz spectrometer. NMR chemical shifts are quoted in ppm; spectra are referenced to TMS for ^{1}H, $^{13}C\{^{1}H\}$, and 85% H_3PO_4 for $^{31}P\{^{1}H\}$ spectra.

IR spectroscopy. FT-IR spectra were recorded on a Mattson Infinity Gold FTIR spectrometer. In-situ IR data was collected on a ReactIR 4000 (Mettler Toledo) with a silicon in-situ probe (SiComp) and a four-bend arm. The reactor consisted of a specially modified pear – shaped 50-mL Schlenk flask. One side-arm was fitted to a source of N_2, the IR probe was inserted with a Teflon adaptor through the center 24/29 neck, and a second side-arm was fitted with a septum for injection of reagents. All ReactIR 4000 experiments were performed in a similar manner as follows: In a inert atmosphere glove box, the flask was charged with precisely weighed sample of solid $Fe_2(S_2C_2H_4)(CO)_3(PMe_3)$(dppv) (ca. 50 mg) and a magnetic Teflon-coated magnetic stir-bar. After the flask was fitted with septa and removed from the box, 5.0 mL of CH_2Cl_2 was added through the middle septum, with care to rinse the sample into the bottom of the flask. The ReactIR probe was then inserted under a purge of N_2 gas. An initial IR spectrum was recorded over the range 4400 – 650 cm^{-1}. The flask was immersed in a slush of MeCN (m.p. -45 °C) on a magnetic stir-plate. After allowing the reactor to thermally equilibrate for several minutes, the IR spectrum was re-recorded. The remainder of the experiment varied depending upon the experiment that was being preformed.

Electrochemistry. Cyclic voltammetry was preformed on a BAS CV-50W Voltammetric Analyzer. The following conditions were observed:

0.1M NBu_4PF_6 (Aldrich) as the supporting electrolyte

glassy carbon as working electrode

Ag/AgCl in saturated KCl as working electrode

Pt wire as counter electrode.

Analyte concentration 10^{-3} M.

EPR Spectroscopy. X-band EPR spectra were collected on a Varian E-122 spectrometer. The samples were recorded at 15 K using an Air Products Helitran cryostat with liquid helium. The magnetic fields were calibrated with a Varian NMR Gaussmeter and the frequency measured with an EIP frequency meter. The polycrystalline sample was flame-sealed under vacuum in a 3 x 4 mm quartz tube at liquid nitrogen temperatures.

II. Electrochemical and Spectroscopic Data.

Figure 1S. Cyclic voltammetry of 10^{-3} M $Fe_2(S_2C_2H_4)(CO)_3(PMe_3)(dppv)$ in CH_2Cl_2 solution over the potential ranges +1500 to -500 mV and +500 to -500 mV. Scan Rate : 50 mV/s. Other conditions: see Electrochemistry section above.

Figure 2S. Cyclic voltammetry of 10^{-3} M $Fe_2(S_2C_2H_4)(CO)_3(PMe_3)(dppv)$ in CH_2Cl_2 solution under a N_2 atmosphere, over the potential range of +500 to -500 mV, with scan rates from 50 to 500 mV/s. Other conditions: see Electrochemistry section above.

Table 1S. $E_{½}$ values recorded by cyclic voltammetry for a 10^{-3}M $Fe_2(S_2C_2H_4)(CO)_3(PMe_3)(dppv)$ in CH_2Cl_2 under N_2 with the potential range of +500 mV to -500 mV for various scan rates.

Figure 3S. Cyclic voltammetry of 10^{-3} M $Fe_2(S_2C_2H_4)(CO)_3(PMe_3)(dppv)$ in CH_2Cl_2 solution under a CO atmosphere with the potential range of +800 to -600mV and +200 to -600 mV. Other conditions: see Electrochemistry section above.

Figure 4S. Cyclic voltammetry of 10^{-3} M $Fe_2(S_2C_2H_4)(CO)_3(PMe_3)(dppv)$ in CH_2Cl_2 solution under a CO atmosphere with the potential range of +800 to -600mV with scan rates from 50 mV/s to 500 mV./s. Other conditions see Electrochemistry section above.

Figure 5S. IR experiment probing reversible binding of CO. Bottom spectrum: $[Fe_2(S_2C_2H_4)(CO)_3(PMe_3)(dppv)]BF_4$ in CH_2Cl_2 solution at -40 °C. Middle spectrum: Addition of 1 atm. CO to the same solution, still at -40 °C. Top spectrum: The same solution after purging with N_2 resulting for 30 min at 0 °C.

Figure 6S. X-band EPR spectrum of polycrystalline $[Fe_2(S_2C_2H_4)(CO)_3(PMe_3)(dppv)]BF_4$ at 15 K. The signal at ~2.05 is attributed to an impurity.

Figure 7S. IR spectrum of $[Fe_2(S_2C_2H_4)(\mu\text{-}CO)(CO)_3(PMe_3)(dppv)](BF_4)_2$ in CH_2Cl_2 solution.

Figure 8S. 202 MHz ^{31}P NMR spectrum of $[Fe_2(S_2C_2H_4)(\mu\text{-}CO)(CO)_3(PMe_3)(dppv)](BF_4)_2$ in CD_2Cl_2 solution at 20 °C. The doublet at δ 68.0 ($J_{P\text{-}P}$ = 3 Hz) is assigned to the dppv ligand and the triplet at δ 38.2 ($J_{P\text{-}P}$ = 3 Hz) is assigned to *P*Me_3.

Figure 9S. IR spectrum of $[Fe_2(S_2C_2H_4)(CO)_2(NO)(PMe_3)(dppv)]BF_4$ in CH_2Cl_2 solution.

Figure 10S. 202 MHz ^{31}P NMR spectrum of $[Fe_2(S_2C_2H_4)(CO)_2(NO)(PMe_3)(dppv)]BF_4$ in CD_2Cl_2 solution at 20 °C. The singlet at δ 74.1 is assigned to the dppv ligand, and the singlet at δ 25.0 is assigned to *P*Me_3.

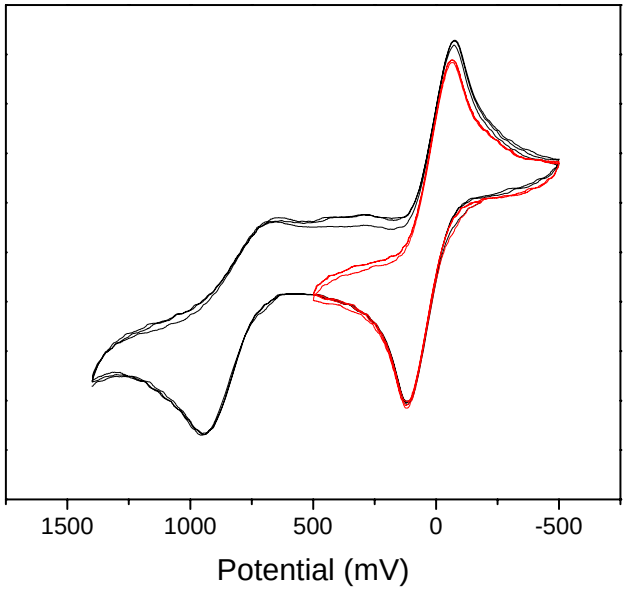

Figure 1S. Cyclic voltammetry of 10^{-3} M $Fe_2(S_2C_2H_4)(CO)_3(PMe_3)(dppv)$ in CH_2Cl_2 solution over the potential ranges +1500 to -500 mV and +500 to -500 mV. Scan Rate : 50 mV/s. Other conditions: see Electrochemistry section above.

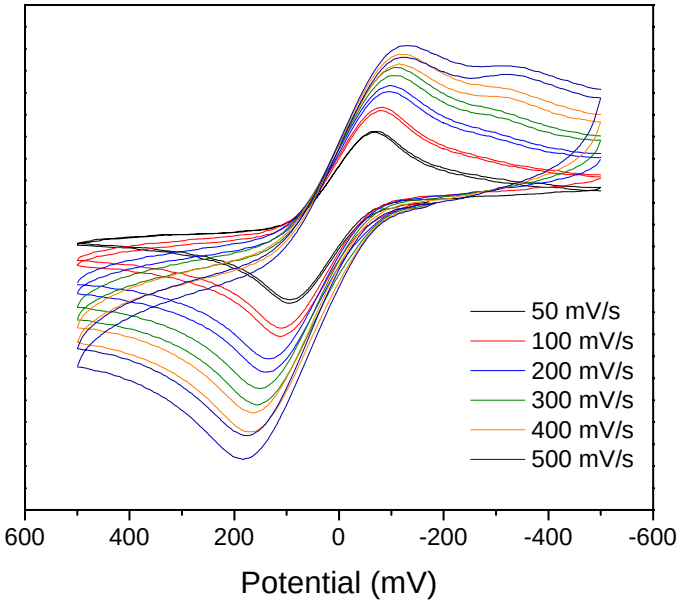

Figure 2S. Cyclic voltammetry of 10^{-3} M $Fe_2(S_2C_2H_4)(CO)_3(PMe_3)(dppv)$ in CH_2Cl_2 solution under a N_2 atmosphere, over the potential range of +500 to -500 mV, with scan rates from 50 to 500 mV/s. Other conditions: see Electrochemistry section above.

Scan Rate	E ½ (mV)
50	+20
100	+20
200	+20
300	+20
400	+25
500	+25

Table 1S. $E_{½}$ values recorded by cyclic voltammetry for a 10^{-3}M $Fe_2(S_2C_2H_4)(CO)_3(PMe_3)(dppv)$ in CH_2Cl_2 under N_2 with the potential range of +500 mV to -500 mV for various scan rates.

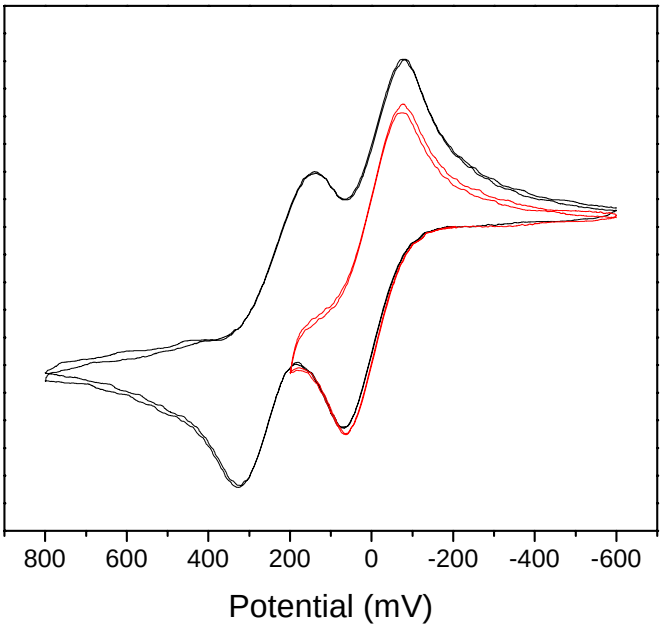

Figure 3S. Cyclic voltammetry of 10^{-3} M $Fe_2(S_2C_2H_4)(CO)_3(PMe_3)(dppv)$ in CH_2Cl_2 solution under a CO atmosphere with the potential range of +800 to -600mV and +200 to -600 mV. Other conditions: see Electrochemistry section above.

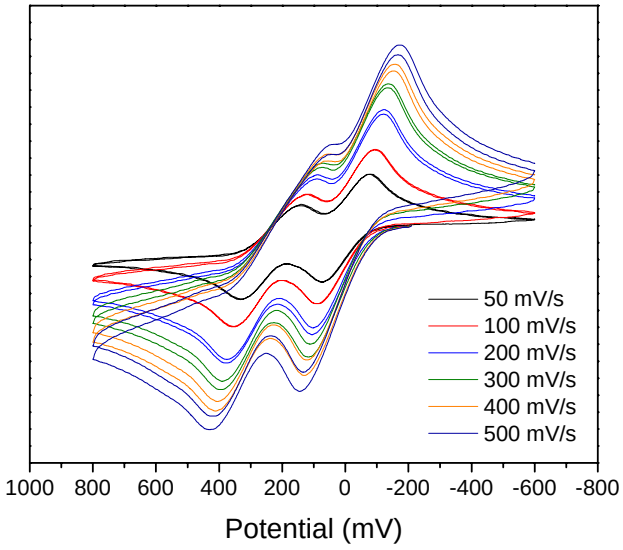

Figure 4S. Cyclic voltammetry of 10^{-3} M $Fe_2(S_2C_2H_4)(CO)_3(PMe_3)(dppv)$ in CH_2Cl_2 solution under 1 atm. CO over the potential range of +800 to -600mV with scan rates from 50 mV/s to 500 mV./s. Other conditions: see Electrochemistry section above.

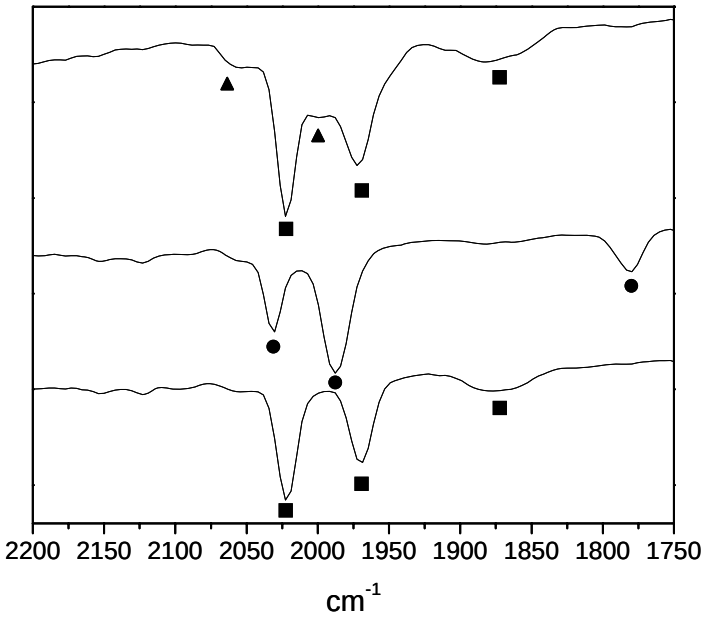

Figure 5S. IR experiment probing reversible binding of CO. Bottom spectrum: $[Fe_2(S_2C_2H_4)(CO)_3(PMe_3)(dppv)]BF_4$ in CH_2Cl_2 solution at -40 °C. Middle spectrum: Addition of 1 atm. CO to the same solution, still at -40 °C. Top spectrum: The same solution after purging with N_2 for 30 min at 0 °C.

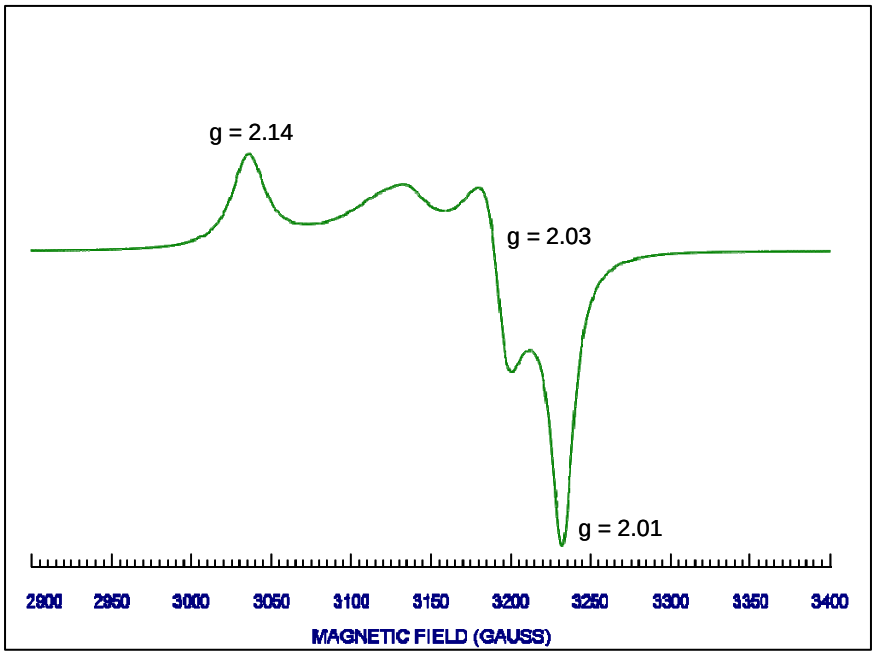

Figure 6S. X-band EPR spectrum of polycrystalline $[Fe_2(S_2C_2H_4)(CO)_3(PMe_3)(dppv)]BF_4$ at 15 K. The signal at ~2.05 is attributed to an impurity.

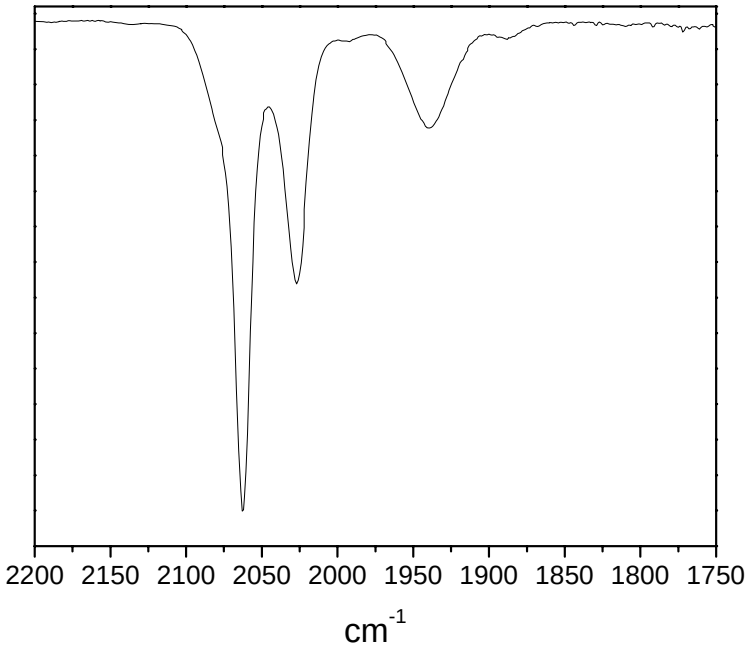

Figure 7S. IR spectrum of $[Fe_2(S_2C_2H_4)(\mu\text{-}CO)(CO)_3(PMe_3)(dppv)](BF_4)_2$ in CH_2Cl_2 solution.

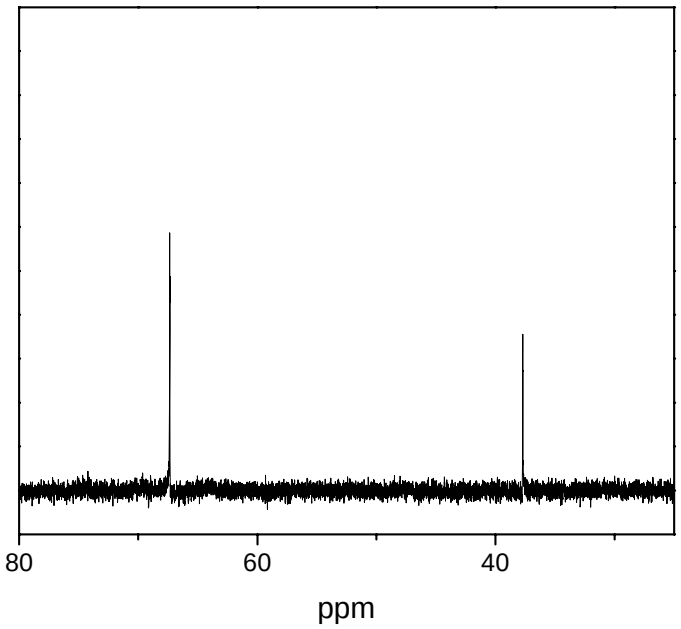

Figure 8S. 202 MHz ^{31}P NMR spectrum of $[Fe_2(S_2C_2H_4)(\mu\text{-}CO)(CO)_3(PMe_3)(dppv)](BF_4)_2$ in CD_2Cl_2 solution at 20 °C. The doublet at δ 68.0 ($J_{P\text{-}P}$ = 3 Hz) is assigned to the dppv ligand and the triplet at δ 38.2 ($J_{P\text{-}P}$ = 3 Hz) is assigned to *P*Me_3.

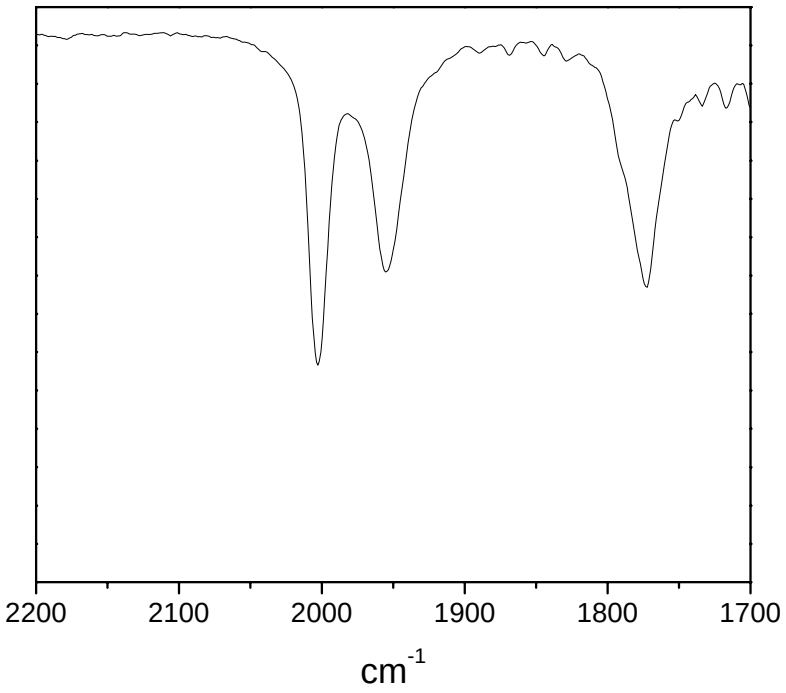

Figure 9S. IR spectrum of $[Fe_2(S_2C_2H_4)(CO)_2(NO)(PMe_3)(dppv)]BF_4$ in CH_2Cl_2 solution.

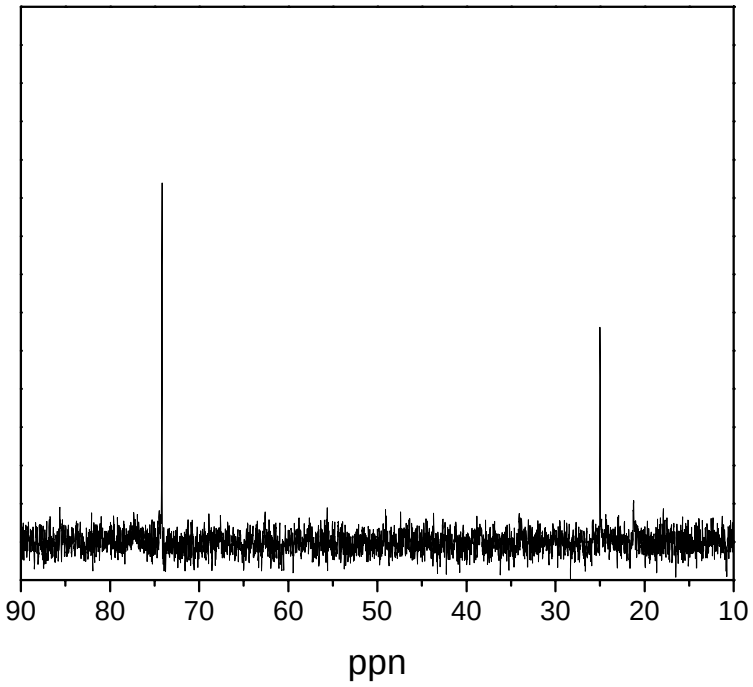

Figure 10S. 202 MHz ^{31}P NMR spectrum of $[Fe_2(S_2C_2H_4)(CO)_2(NO)(PMe_3)(dppv)]BF_4$ in CD_2Cl_2 solution at 20 °C. The singlet at δ 74.1 is assigned to the dppv ligand, and the singlet at δ 25.0 is assigned to *P*Me_3.

III. Crystallography.

Crystals were mounted to a thin glass fiber using Paratone-N oil (Exxon). Data, collected at 198 K on a Siemens CCD diffractometer, were filtered to remove statistical outliers. The integration software (SAINT) was used to test for crystal decay as a bi-linear function of X-ray exposure time and sin(Θ). The data were solved using SHELXTL by Direct Methods (Table 1); atomic positions were deduced from an E map or by an unweighted difference Fourier synthesis. H atom U's were assigned as $1.2U_{eq}$ for adjacent C atoms. Non-H atoms were refined anisotropically. Successful convergence of the full-matrix least-squares refinement of F^2 was indicated by the maximum shift/error for the final cycle.

Table 2. Details of Data Collection and Structure Refinement for Crystallography.

Complex	[**1**]BF_4
Chemical formula	$C_{34}H_{35}BF_4Fe_2O_3P_3S_2$
Temperature (K)	193 (2)
Crystal size (mm^3)	0.53 x 0.28 x 0.06
Crystal system	Orthorhombic
Space group	Pnma
A (Å)	23.0921 (8)
B (Å)	18.2932 (6)
C (Å)	8.5353 (3)
α (^{o})	90
β (^{o})	90
γ (^{o})	90
V ($Å^3$)	3605.6 (2)
Z	4
Density calcd (Mg m^{-3})	1.561
μ (Mo Kα, mm^{-1})	0.71073
max./min. trans'n	0.9374/0.7048
reflections meas'd/Indep.	62694/4911
data/restraints/parameters	4911/37/253
GOF on F^2	1.053
Rint	0.0363
R1 [I > 2σ] (all data)[a]	0.0339 (0.0916)
wR2 [I > 2σ] (all data)[b]	0.0430 (0.0981)
max. peak/hole ($e^-/Å^3$)	0.591 / -0.539

[a] $R1 = \Sigma||F_o|-|F_c||/\Sigma|F_o|$

[b] $wR2 = \{[w(|F_o|-|F_c|)^2]/\Sigma[wF_o^2]\}^{1/2}$, where $w = 1/\sigma^2 (F_o)$

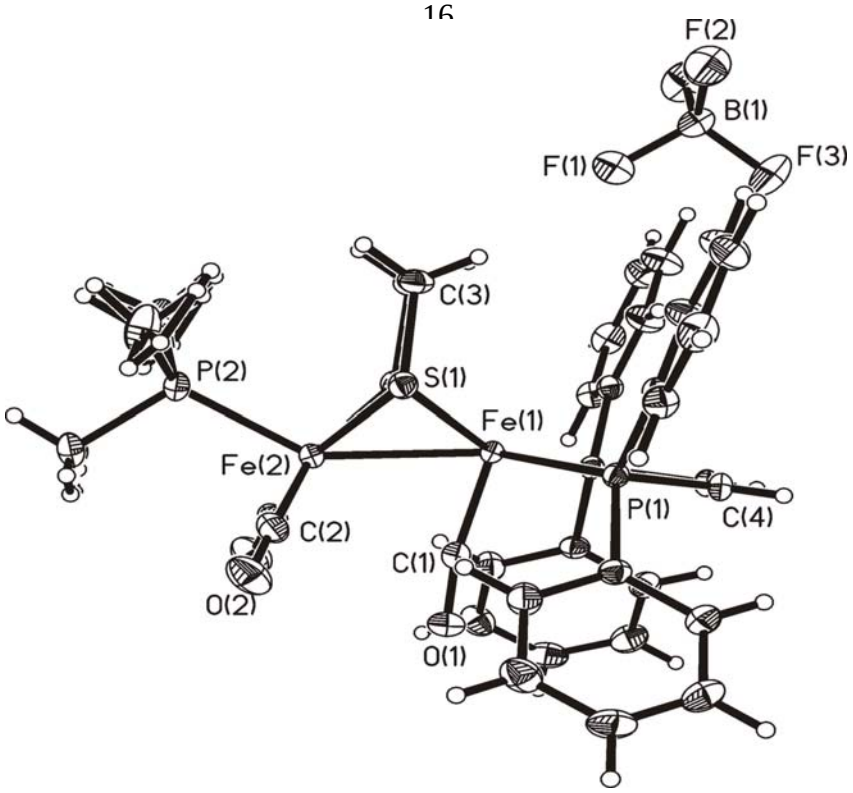

Figure 6S. Structure of $[Fe_2(S_2C_2H_4)(CO)_3(PMe_3)(dppv)]BF_4$ with the thermal ellipsoids set at 35 %.

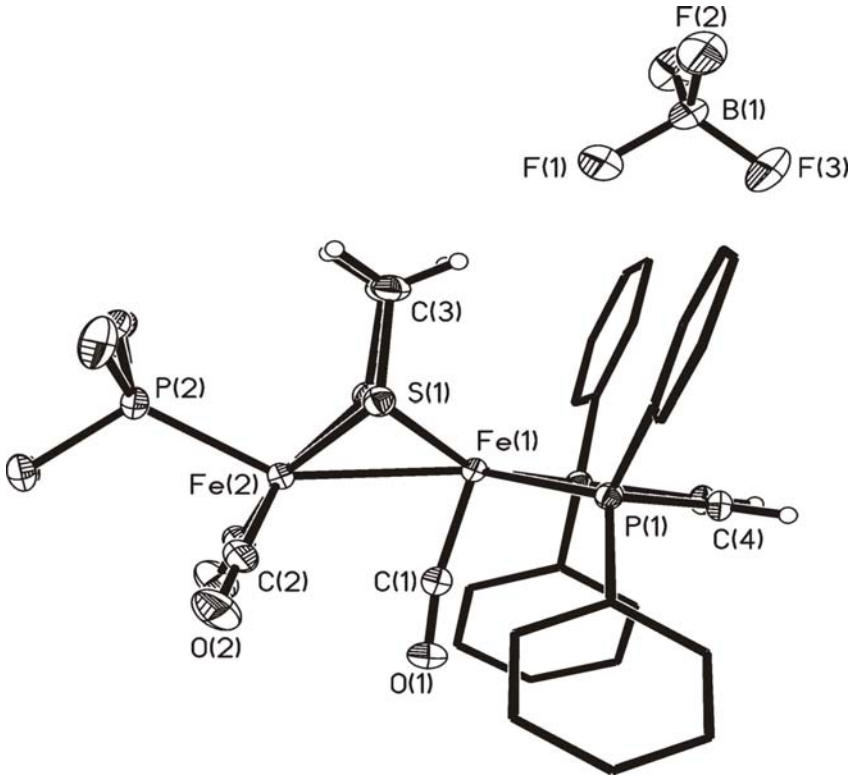

Figure 7S. Structure of $[Fe_2(S_2C_2H_4)(CO)_3(PMe_3)(dppv)]BF_4$ with the thermal ellipsoids set at 35 %. Phenyl ellipsoids and hydrogen atoms have been omitted for clarity.

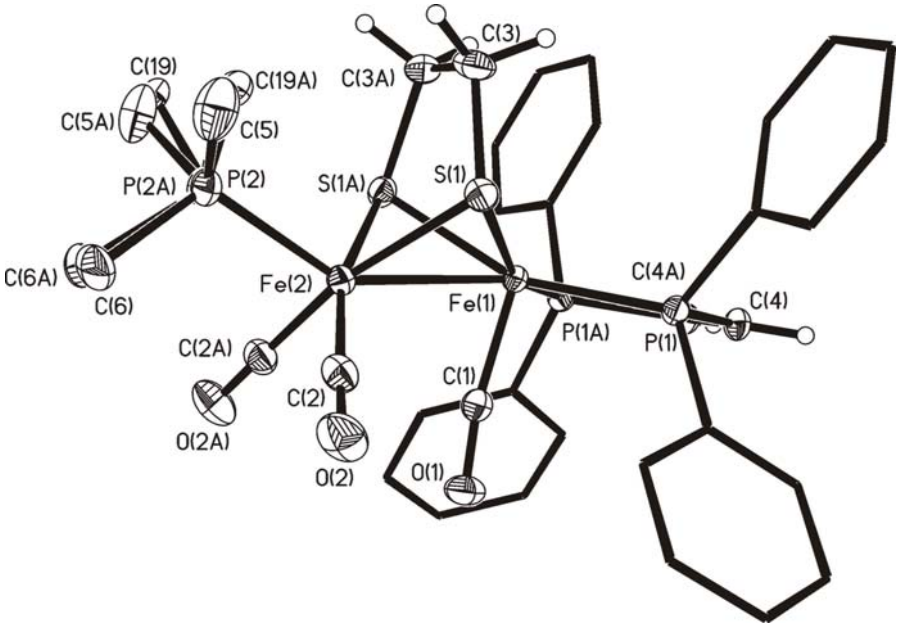

Figure 8S. Structure of the cation in $[Fe_2(S_2C_2H_4)(CO)_3(PMe_3)(dppv)]BF_4$ with the thermal ellipsoids set at 35 %. Phenyl ellipsoids and hydrogen atoms have been omitted for clarity.

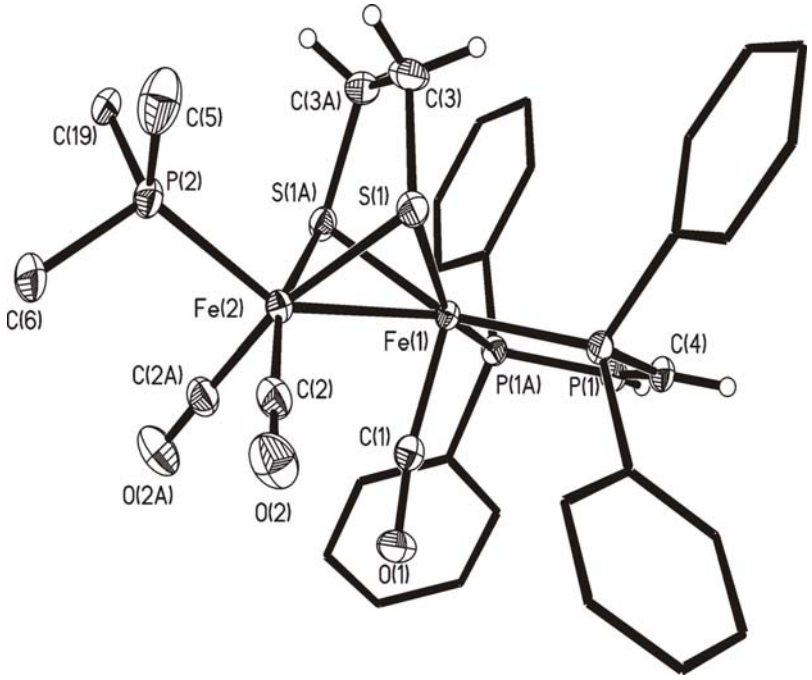

Figure XS. Structure of the cation in $[Fe_2(S_2C_2H_4)(CO)_3(PMe_3)(dppv)]BF_4$ with the thermal ellipsoids set at 35 %. One of the two orientations of the PMe_3 ligand is shown. Phenyl ellipsoids and hydrogen atoms have been omitted for clarity.

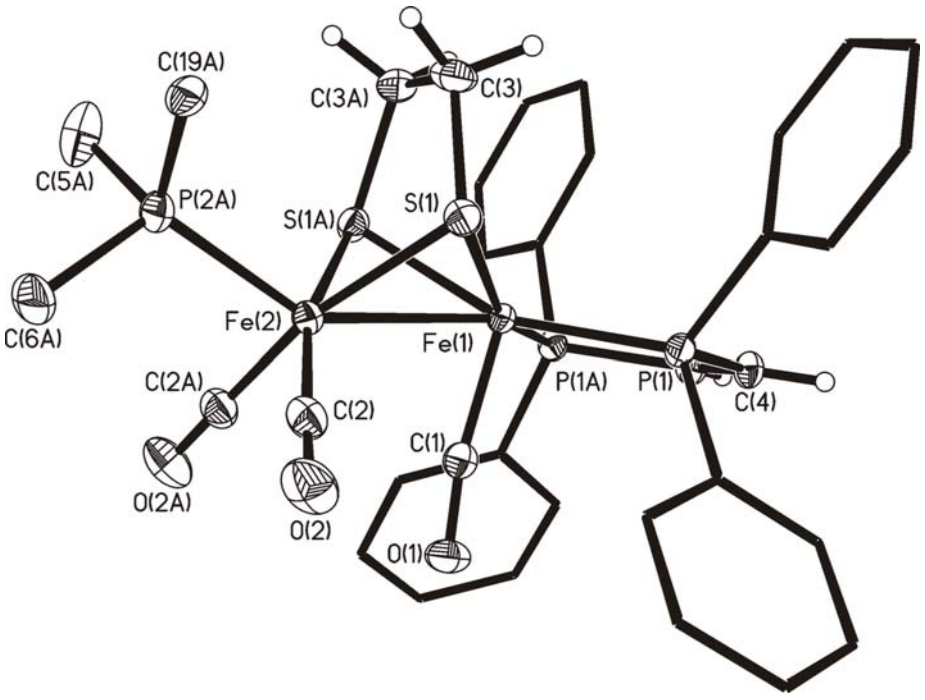

Figure XS. Structure of the cation in $[Fe_2(S_2C_2H_4)(CO)_3(PMe_3)(dppv)]BF_4$ with the thermal ellipsoids set at 35 %. One of the two orientations of the PMe_3 ligand is shown. Phenyl ellipsoids and hydrogen atoms have been omitted for clarity.

Table 3. Atomic coordinates (x 10^4) and equivalent isotropic displacement parameters ($Å^2$ x 10^2) for $[Fe_2(S_2C_2H_4)(CO)_3(PMe_3)(dppv)]BF_4$. U_{eq} is defined as one third of the trace of the orthogonalized U_{ij} tensor.

	x	y	z	U(eq)
Fe(1)	666(1)	2500	1336(1)	19(1)
Fe(2)	-370(1)	2500	2406(1)	24(1)
S(1)	315(1)	1695(1)	3130(1)	26(1)
P(1)	1250(1)	1662(1)	287(1)	22(1)
P(2)	-948(1)	2535(6)	4484(1)	32(1)
F(1)	2126(1)	2500	5663(3)	62(1)
F(2)	2850(1)	1889(1)	6829(2)	62(1)
F(3)	3004(1)	2500	4544(3)	64(1)
O(1)	-60(1)	2500	-1467(3)	41(1)
O(2)	-1012(1)	1328(1)	846(2)	53(1)
C(1)	182(1)	2500	-288(3)	28(1)
C(2)	-772(1)	1787(1)	1459(3)	34(1)
C(3)	671(1)	2086(1)	4852(2)	37(1)
C(4)	1844(1)	2137(1)	-660(2)	27(1)
C(5)	-963(5)	1723(8)	5674(13)	58(3)
C(19)	-835(4)	3277(6)	5851(10)	31(1)
C(6)	-1706(2)	2657(5)	4028(6)	57(3)
C(7)	957(1)	1063(1)	-1225(2)	26(1)
C(8)	1293(1)	833(1)	-2490(2)	34(1)
C(9)	1067(1)	344(1)	-3572(3)	43(1)
C(10)	512(1)	84(1)	-3403(3)	43(1)
C(11)	174(1)	310(1)	-2171(3)	42(1)
C(12)	395(1)	802(1)	-1076(3)	36(1)
C(13)	1632(1)	1023(1)	1568(2)	26(1)
C(14)	1559(1)	269(1)	1466(2)	32(1)
C(15)	1870(1)	-194(1)	2430(3)	40(1)
C(16)	2256(1)	80(2)	3503(3)	43(1)
C(17)	2333(1)	833(2)	3626(3)	47(1)
C(18)	2018(1)	1302(1)	2667(3)	38(1)
B(1)	2721(2)	2500	5953(4)	37(1)

Table 4. Bond lengths (Å) and angles (°) for $[Fe_2(S_2C_2H_4)(CO)_3(PMe_3)(dppv)]BF_4$.

Fe(1)-C(1)	1.781(3)
Fe(1)-P(1)	2.2302(5)
Fe(1)-P(1)#1	2.2302(5)
Fe(1)-S(1)#1	2.2742(5)
Fe(1)-S(1)	2.2742(5)
Fe(1)-Fe(2)	2.5598(5)
Fe(2)-C(2)	1.793(2)
Fe(2)-C(2)#1	1.793(2)
Fe(2)-P(2)#1	2.2218(10)
Fe(2)-P(2)	2.2218(10)
Fe(2)-S(1)	2.2474(6)
Fe(2)-S(1)#1	2.2474(6)
S(1)-C(3)	1.831(2)
P(1)-C(4)	1.8122(19)
P(1)-C(7)	1.823(2)
P(1)-C(13)	1.827(2)
P(2)-C(5)#1	1.695(18)
P(2)-C(5)	1.799(6)
P(2)-C(6)	1.806(4)
P(2)-C(19)	1.808(6)
P(2)-C(6)#1	1.826(5)
P(2)-C(19)#1	1.907(16)
F(1)-B(1)	1.396(5)
F(2)-B(1)	1.378(3)
F(3)-B(1)	1.369(4)
O(1)-C(1)	1.151(3)
O(2)-C(2)	1.136(3)
C(3)-C(3)#1	1.514(5)
C(3)-H(3A)	0.9900
C(3)-H(3B)	0.9900
C(4)-C(4)#1	1.328(4)
C(4)-H(4)	0.9500
C(5)-H(5A)	0.9800
C(5)-H(5B)	0.9800

C(5)-H(5C)	0.9800
C(19)-H(19A)	0.9800
C(19)-H(19B)	0.9800
C(19)-H(19C)	0.9800
C(6)-H(6A)	0.9800
C(6)-H(6B)	0.9800
C(6)-H(6C)	0.9800
C(7)-C(12)	1.389(3)
C(7)-C(8)	1.394(3)
C(8)-C(9)	1.388(3)
C(8)-H(8)	0.9500
C(9)-C(10)	1.374(4)
C(9)-H(9)	0.9500
C(10)-C(11)	1.374(4)
C(10)-H(10)	0.9500
C(11)-C(12)	1.394(3)
C(11)-H(11)	0.9500
C(12)-H(12)	0.9500
C(13)-C(18)	1.389(3)
C(13)-C(14)	1.393(3)
C(14)-C(15)	1.382(3)
C(14)-H(14)	0.9500
C(15)-C(16)	1.373(4)
C(15)-H(15)	0.9500
C(16)-C(17)	1.392(4)
C(16)-H(16)	0.9500
C(17)-C(18)	1.392(3)
C(17)-H(17)	0.9500
C(18)-H(18)	0.9500
B(1)-F(2)#1	1.378(3)

C(1)-Fe(1)-P(1)	93.87(7)
C(1)-Fe(1)-P(1)#1	93.87(7)
P(1)-Fe(1)-P(1)#1	86.84(3)
C(1)-Fe(1)-S(1)#1	107.47(7)
P(1)-Fe(1)-S(1)#1	158.65(2)

P(1)#1-Fe(1)-S(1)#1	92.339(18)
C(1)-Fe(1)-S(1)	107.47(7)
P(1)-Fe(1)-S(1)	92.340(18)
P(1)#1-Fe(1)-S(1)	158.65(2)
S(1)#1-Fe(1)-S(1)	80.76(3)
C(1)-Fe(1)-Fe(2)	72.02(9)
P(1)-Fe(1)-Fe(2)	135.130(14)
P(1)#1-Fe(1)-Fe(2)	135.130(14)
S(1)#1-Fe(1)-Fe(2)	55.027(15)
S(1)-Fe(1)-Fe(2)	55.027(15)
C(2)-Fe(2)-C(2)#1	93.28(14)
C(2)-Fe(2)-P(2)#1	91.6(2)
C(2)#1-Fe(2)-P(2)#1	94.0(2)
C(2)-Fe(2)-P(2)	94.0(2)
C(2)#1-Fe(2)-P(2)	91.6(2)
P(2)#1-Fe(2)-P(2)	3.3(6)
C(2)-Fe(2)-S(1)	90.65(7)
C(2)#1-Fe(2)-S(1)	164.73(8)
P(2)#1-Fe(2)-S(1)	100.6(2)
P(2)-Fe(2)-S(1)	102.9(2)
C(2)-Fe(2)-S(1)#1	164.73(8)
C(2)#1-Fe(2)-S(1)#1	90.65(7)
P(2)#1-Fe(2)-S(1)#1	102.9(2)
P(2)-Fe(2)-S(1)#1	100.6(2)
S(1)-Fe(2)-S(1)#1	81.93(3)
C(2)-Fe(2)-Fe(1)	108.82(7)
C(2)#1-Fe(2)-Fe(1)	108.82(7)
P(2)#1-Fe(2)-Fe(1)	147.86(3)
P(2)-Fe(2)-Fe(1)	147.86(3)
S(1)-Fe(2)-Fe(1)	56.016(15)
S(1)#1-Fe(2)-Fe(1)	56.016(15)
C(3)-S(1)-Fe(2)	106.29(8)
C(3)-S(1)-Fe(1)	97.28(7)
Fe(2)-S(1)-Fe(1)	68.958(18)
C(4)-P(1)-C(7)	104.66(9)
C(4)-P(1)-C(13)	102.05(9)

C(7)-P(1)-C(13)	102.62(9)
C(4)-P(1)-Fe(1)	107.88(7)
C(7)-P(1)-Fe(1)	118.21(7)
C(13)-P(1)-Fe(1)	119.42(6)
C(5)-P(2)-C(6)	101.9(4)
C(5)-P(2)-C(19)	105.0(2)
C(6)-P(2)-C(19)	100.7(4)
C(5)#1-P(2)-Fe(2)	120.9(7)
C(5)-P(2)-Fe(2)	116.0(5)
C(6)-P(2)-Fe(2)	114.45(16)
C(19)-P(2)-Fe(2)	116.7(4)
C(6)#1-P(2)-Fe(2)	113.6(2)
C(19)#1-P(2)-Fe(2)	112.6(5)
O(1)-C(1)-Fe(1)	170.1(3)
O(2)-C(2)-Fe(2)	178.1(2)
C(3)#1-C(3)-S(1)	113.04(8)
C(3)#1-C(3)-H(3A)	109.0
S(1)-C(3)-H(3A)	109.0
C(3)#1-C(3)-H(3B)	109.0
S(1)-C(3)-H(3B)	109.0
H(3A)-C(3)-H(3B)	107.8
C(4)#1-C(4)-P(1)	118.65(6)
C(4)#1-C(4)-H(4)	120.7
P(1)-C(4)-H(4)	120.7
P(2)-C(5)-H(5A)	109.5
P(2)-C(5)-H(5B)	109.5
H(5A)-C(5)-H(5B)	109.5
P(2)-C(5)-H(5C)	109.5
H(5A)-C(5)-H(5C)	109.5
H(5B)-C(5)-H(5C)	109.5
P(2)-C(19)-H(19A)	109.5
P(2)-C(19)-H(19B)	109.5
H(19A)-C(19)-H(19B)	109.5
P(2)-C(19)-H(19C)	109.5
H(19A)-C(19)-H(19C)	109.5
H(19B)-C(19)-H(19C)	109.5

P(2)-C(6)-H(6A)	109.5
P(2)-C(6)-H(6B)	109.5
H(6A)-C(6)-H(6B)	109.5
P(2)-C(6)-H(6C)	109.5
H(6A)-C(6)-H(6C)	109.5
H(6B)-C(6)-H(6C)	109.5
C(12)-C(7)-C(8)	119.11(19)
C(12)-C(7)-P(1)	119.24(15)
C(8)-C(7)-P(1)	121.58(16)
C(9)-C(8)-C(7)	120.1(2)
C(9)-C(8)-H(8)	120.0
C(7)-C(8)-H(8)	120.0
C(10)-C(9)-C(8)	120.3(2)
C(10)-C(9)-H(9)	119.9
C(8)-C(9)-H(9)	119.9
C(9)-C(10)-C(11)	120.4(2)
C(9)-C(10)-H(10)	119.8
C(11)-C(10)-H(10)	119.8
C(10)-C(11)-C(12)	120.0(2)
C(10)-C(11)-H(11)	120.0
C(12)-C(11)-H(11)	120.0
C(7)-C(12)-C(11)	120.2(2)
C(7)-C(12)-H(12)	119.9
C(11)-C(12)-H(12)	119.9
C(18)-C(13)-C(14)	118.85(19)
C(18)-C(13)-P(1)	118.63(16)
C(14)-C(13)-P(1)	122.51(16)
C(15)-C(14)-C(13)	120.5(2)
C(15)-C(14)-H(14)	119.8
C(13)-C(14)-H(14)	119.8
C(16)-C(15)-C(14)	120.6(2)
C(16)-C(15)-H(15)	119.7
C(14)-C(15)-H(15)	119.7
C(15)-C(16)-C(17)	119.7(2)
C(15)-C(16)-H(16)	120.2
C(17)-C(16)-H(16)	120.2

C(18)-C(17)-C(16)	119.9(2)
C(18)-C(17)-H(17)	120.1
C(16)-C(17)-H(17)	120.1
C(13)-C(18)-C(17)	120.5(2)
C(13)-C(18)-H(18)	119.8
C(17)-C(18)-H(18)	119.8
F(3)-B(1)-F(2)#1	111.9(2)
F(3)-B(1)-F(2)	111.9(2)
F(2)#1-B(1)-F(2)	108.5(3)
F(3)-B(1)-F(1)	108.3(3)
F(2)#1-B(1)-F(1)	108.0(2)
F(2)-B(1)-F(1)	108.0(2)

Symmetry transformations used to generate equivalent atoms:
#1 x,-y+1/2,z

Table 5. Anisotropic displacement parameters ($Å^2 x10^3$) for $[Fe_2(S_2C_2H_4)(CO)_3(PMe_3)(dppv)]BF_4$. The anisotropic displacement factor exponent takes the form: $-2\pi^2[h^2 a^{*2}U^{11} + ... + 2 h k a^* b^* U^{12}]$

	U^{11}	U^{22}	U^{33}	U^{23}	U^{13}	U^{12}
Fe(1)	18(1)	22(1)	18(1)	0	2(1)	0
Fe(2)	18(1)	31(1)	24(1)	0	0(1)	0
S(1)	25(1)	27(1)	27(1)	5(1)	2(1)	0(1)
P(1)	21(1)	23(1)	22(1)	-2(1)	2(1)	1(1)
P(2)	23(1)	41(2)	30(1)	-2(2)	6(1)	-1(1)
F(1)	46(1)	90(2)	50(1)	0	-8(1)	0
F(2)	76(1)	52(1)	59(1)	16(1)	9(1)	21(1)
F(3)	76(2)	69(2)	46(1)	0	27(1)	0
O(1)	39(1)	56(2)	27(1)	0	-8(1)	0
O(2)	43(1)	47(1)	70(1)	-12(1)	-15(1)	-8(1)
C(1)	26(1)	30(1)	27(1)	0	2(1)	0
C(2)	26(1)	38(1)	38(1)	1(1)	-3(1)	-1(1)
C(3)	34(1)	51(1)	27(1)	9(1)	-8(1)	-3(1)
C(4)	20(1)	34(1)	28(1)	-2(1)	5(1)	1(1)
C(5)	55(5)	48(4)	71(6)	6(4)	28(4)	-5(4)
C(19)	30(3)	39(3)	25(2)	-5(2)	6(2)	3(2)
C(6)	22(2)	104(8)	46(2)	-12(3)	4(2)	3(3)
C(7)	30(1)	26(1)	24(1)	-3(1)	-3(1)	2(1)
C(8)	38(1)	37(1)	29(1)	-5(1)	2(1)	2(1)
C(9)	57(2)	41(1)	31(1)	-11(1)	3(1)	3(1)
C(10)	59(2)	34(1)	37(1)	-10(1)	-15(1)	2(1)
C(11)	38(1)	37(1)	50(1)	-9(1)	-8(1)	-6(1)
C(12)	32(1)	37(1)	39(1)	-10(1)	2(1)	-3(1)
C(13)	24(1)	28(1)	26(1)	-1(1)	2(1)	5(1)
C(14)	34(1)	28(1)	33(1)	-2(1)	0(1)	1(1)
C(15)	48(1)	26(1)	45(1)	3(1)	7(1)	7(1)
C(16)	40(1)	45(1)	44(1)	8(1)	-4(1)	15(1)
C(17)	46(1)	47(2)	49(1)	2(1)	-20(1)	3(1)
C(18)	41(1)	30(1)	42(1)	-2(1)	-13(1)	1(1)
B(1)	47(2)	35(2)	28(2)	0	4(1)	0

Table 6. Hydrogen coordinates (x 10^4) and isotropic displacement parameters (Å^{2}x 10^3) for $[Fe_2(S_2C_2H_4)(CO)_3(PMe_3)(dppv)]BF_4$.

	x	y	z	U(eq)
H(3A)	472	1910	5808	45
H(3B)	1077	1910	4892	45
H(4)	2148	1872	-1146	33
H(5A)	-1201	1811	6605	87
H(5B)	-568	1599	5997	87
H(5C)	-1127	1318	5068	87
H(19A)	-892	3745	5312	47
H(19B)	-440	3252	6267	47
H(19C)	-1113	3236	6715	47
H(6A)	-1824	2295	3243	86
H(6B)	-1768	3150	3612	86
H(6C)	-1937	2591	4980	86
H(8)	1676	1012	-2613	41
H(9)	1297	188	-4432	51
H(10)	362	-255	-4143	52
H(11)	-210	132	-2065	50
H(12)	161	959	-226	43
H(14)	1293	71	730	38
H(15)	1816	-708	2349	47
H(16)	2469	-242	4159	52
H(17)	2600	1026	4364	57
H(18)	2066	1815	2764	46